SiC generation mechanism in photovoltaic crystal pulling waste graphite infusion cylinder

Yiyou Hu
Kunming University of Science and Technology
Zhengjie Chen
czjkmust@126.com
Kunming University of Science and Technology
Yonghang Zhang
Kunming University of Science and Technology
Xiuhua Chen
Yunnan University
Wenhui Ma
Kunming University of Science and Technology

Research Article

Keywords: Photovoltaic crystal pulling, graphite, SiC, infusion cylinder

Posted Date: November 9th, 2023

DOI: https://doi.org/10.21203/rs.3.rs-3562745/v1

Additional Declarations: No competing interests reported.

Version of Record: A version of this preprint was published at Silicon on February 19th, 2024. See the published version at https://doi.org/10.1007/s12633-024-02888-y.

SiC generation mechanism in photovoltaic crystal pulling waste graphite infusion cylinder

Yiyou Hu[1,2], Zhengjie Chen[1,2,3*], Yonghang Zhang[1,2,3], Xiuhua Chen[4], Wenhui Ma[1,2,3]

[1] Faculty of Metallurgical and Energy Engineering, Kunming University of Science and Technology, Kunming 650093, China;

[2] State Key Laboratory of Complex Nonferrous Metal Resources Cleaning Utilization in Yunnan Province, Kunming University of Science and Technology, Kunming 650093, China;

[3] The National Engineering Laboratory for Vacuum Metallurgy, Kunming University of Science and Technology, Kunming 650093, China;

[4] The School of Materials and Energy, Yunnan University, Kunming 650093, China;

*Corresponding author

E-mail address: czjkmust@126.com(Z. Chen)

Abstract

Carbon etching and silicide deposition are common phenomena in furnaces during photovoltaic crystal pulling processes,both of which decrease Graphite components in the furnace service life and pollute silicon-based materials. SiC as one of the major silicides and carbon etching products whose generation mechanism is of practical significance. Therefore, this study took discarded graphite infusion cylinders with significantly different apparent morphologies as the research objects. Through systematic characterization and thermodynamic analysis, we investigated the physical and chemical reactions that occurred during the generation of SiC in various regions of a discarded graphite infusion cylinder. We derived the SiC delamination, infiltration, and phagocytosis mechanism to explain the formation of the apparent morphological characteristics of the waste graphite infusion cylinder. We also described Generation mechanism of SiC in graphite infusion cylinder during photovoltaic crystal pulling process to provide a theoretical basis for prolonging the service life of the graphite infusion cylinder and treating waste graphite infusion cylinder .

Keywords: Photovoltaic crystal pulling, graphite, SiC, infusion cylinder

1. Introduction

The development of a sustainable low-carbon economy and the use of renewable and clean energy are important for reducing carbon emissions26. Photovoltaic (PV) power generation is one of the most promising ways to obtain clean energy [4-6], and China is the world's largest energy consumer and a leader in the solar PV industry[7-9]. The rapid development of the photovoltaic industry[10-11]has led to a rapid growth in demand for industrial silicon, monocrystalline silicon, polycrystalline silicon, chips, cells, and modules[12-14]. Li et al[15]pointed out that graphite products are necessary for the development of the photovoltaic industry, and are often used to manufacture key upstream equipment in the photovoltaic industry[16-18]. However, severe carbon etching and silicide deposition often occur[19-20], which greatly shorten the service life of components and affect the quality of the silicon ingots. This process also generates a large amount of waste graphite, which greatly impacts the development of the photovoltaic industry and pollutes the environment. Because graphite components are made of isostatically-pressed, high-purity graphite, they should be fully recycled[21]. Purifying this waste graphite infusion cylinder or reducing its generation can fully utilize graphite resources and improve industrial efficiency.

In recent years, the generation mechanism of silicon carbide during the manufacture of monocrystalline and polycrystalline silicon has been investigated. Liu et al.[22] performed transient global modeling of heat and mass transfer during the melting of silicon crystal growth in direct-drawn monocrystalline silicon and simulated the formation and engulfment mechanism of silicon carbide during the directional solidification growth of industrial silicon. Kalejs and Chalmers[23] probed the nucleation and growth mechanisms of silicon carbide at the solid-liquid interface. Ouaddah et al.[24]proposed a model for the presence of silicon carbide precipitates at the solid-liquid interface during silicon-based solidification processes . Bornside et al. explored the formation mechanism of silicon-carbon impurities in the system by simulating the convection and diffusion of SiO and CO in the furnace during the

production of monocrystalline silicon by the straight drawing process(CZ). The simulation illustrated that during the direct drawing of monocrystalline silicon, the source of carbon contaminants entered the silicon melt via gas-phase transport, i.e., in the form of carbon monoxide. Dissolved oxygen in the melt and silicon generated by silicon monoxide entered the furnace via evaporation of the surface of the silicon melt. The gas-phase SiO subsequently reacted with the graphite fixed inside the furnace to form CO. Then, this cycle of reactions was repeated, and silicon carbide was also produced during the reaction[25]. During the reaction, the sources of oxygen included the dissolution of the quartz crucible containing molten Si and the absorption of CO into the melt[26], the sources of carbon were the graphite components in the furnace[27-28].

Various studies have established mod els to determine the formation mechanism of SiC during polycrystalline silicon pulling. Delannoy et al.[29] introduced a time-dependent three-dimensional numerical model for the solidification of large-size photovoltaic silicon ingots, which was applicable to account the formation mechanisms of liquid-phase SiC. The proposed SiC formation mechanism was: dissolved carbon aggregated on the surface of the silicon melt, silicon carbide precipitated when the carbon concentration exceeded the carbon dissolution limit of the silicon melt, and then silicon nucleated on the silicon carbide particles and eventually engulfed them to form a sand-like structure. Gao et al.[30]proposed a mechanism for the formation of carbon impurities in the gas phase during polysilicon production. Subsequently, Zheng et al. summarised and proposed the generation, transport and dissolution laws of SiO and CO in the furnace based on the duo's viewpoints, and elaborated on the mechanism by which the carbon solutes overflowed from the cured silicon and piled up at the growth interface to form SiC precipitates[31]. The generation and migration of carbon impurities have been widely studied, and the corresponding mechanism of silicon carbide formation has been proposed. However, due to the the research subjects were in a high-temperature, vacuum, closed environment, the reaction temperature changes with the thermal environment. Current research has mainly focused on the use of computer simulations and theoretical analyses,and the main objects were formation

mechanisms of SiC in silicon melt, monocrystalline silicon and polycrystalline silicon products.There have been fewer reports of the formation mechanism about SiC in photovoltaic crystal pulling waste graphite infusion cylinder.

In this article, the formation mechanism of SiC in a photovoltaic pulling crystal waste graphite infusion cylinder is proposed.Selected the existence of significant differences in the apparent morphology of the photovoltaic crystal pulling waste graphite infusion cylinder as the object of study, through the systematic characterisation and analysis, thermodynamic analysis to study the mechanism of SiC generation in the photovoltaic crystal pulling waste graphite infusion cylinder, with the aim of providing the theoretical basis to increase the service life of photovoltaic crystal pulling graphite infusion cylinder and treatment and purification application of waste graphite infusion cylinders.

2. Material and method

2.1 Sample Preparation

The waste graphite infusion cylinder was placed in a blast drying oven at 70 °C for two hours. After cooling, the sample was divided into six regions according to its apparent morphological characteristics. A part of the sample was selected from each of the six regions for crushing, grinding, and sieving, Fig. 1(a) shows the sample obtained after crushing,which black powder for qualitative and quantitative analyses samples can be prepared by grinding and sieving to obtain by it .Some samples from each of the 6 regions were selected to be cut and polished to obtain a block sample, which Can be used in SEM to observe delamination, infiltration and other morphological features,as shown in Fig. 1(b).

2.2 Sample characterization

According to the GB/T3521-2008 graphite chemical analysis method to detect the fixed carbon content of the sample, each sample was tested three times and the average value was taken. An Agilent 5800 VDV ICP-OES inductively coupled plasma emission spectrometer was used for the qualitative and quantitative analysis of the sample elements. X-ray diffractometer model X'Pert3Powder was used for the material

identification. A PHI5000 Versaprobe-II multifunctional scanning imaging photoelectron spectrometer was used to analyze the chemical states of samples. A VEGA3 TESCAN tungsten filament scanning electron microscope was used to observe the morphology and microstructure of the samples.

3. Results and Discussion

3.1 Characterization of the apparent morphology of the samples

As shown in Fig. 2(a), there were significant differences in the apparent morphology of the waste graphite infusion cylinder, which was divided into six regions from top to bottom: A, B, C, D, E, F. Fig. 2(b) shows that there were different characteristics among the six regions. In region A, there were earthy-yellow and white intertwined substances attached to the surface of the infusion cylinder, which were powdered, lumpy amorphous substances with a fine, soft, and loose texture. In region B, there were a few gray scaly substances on the surface of the graphite body.In region C, the surface of the infusion cylinder generated a more greenish material. The upper layer was granular and light texture while the lower layer was a denser, more massive material. In region D, more black particles accumulated material, and the particle size was large (1–3 mm), and the particle density was higher, with a metallic luster. In region E, substances on the surface of the infusion cylinder were similar to region D, but the particles size were smaller than those in region D, and the color was lighter. In region F, the surface of the infusion cylinder were lighter coloured spherical silver-grey particles with a high degree of adhesion to the infusion cylinder compared to areas D and E,the particles were hard, with a metallic appearance, and the densities were the highest among the six areas. Overall, from area A to area F, the material generated on the surface of the infusion cylinder cylinder gradually hardened and became more metallic.

3.2 Qualitative and quantitative analysis

The fixed carbon detection data are shown in Table 1. Overall, the fixed carbon contents of the waste graphite infusion cylinders were all over 50% because the infusion cylinders were made of high-purity isostatically-pressed graphite. Among the six

regions, A region had the highest fixed carbon content, and B region was slightly lower than region A,but both regions were higher than 90%, probably due to the lowest relative temperature in the A region. Most silicon vapors directly condensed here,which did not react with the graphite body of the infusion cylinders. From region A to F, the fixed carbon content gradually decreased, probably more SiC were produced due to closer proximity to the silicon melt and at higher temperatures.The ICP results also illustrated this point, in which the waste graphite infusion cylinder mainly contained C, Si, Cu, Sn, Fe, and Ti elements, of which the relative content of carbon was the highest, followed by silicon.Relative content of silicon obtained from ICP analysis. From regions A to F, the relative content of silicon gradually increased, indicating that there may be more silicon or silicon carbide in the system. So the XRD was carried out on the ash of the waste graphite infusion cylinder samples, the main phases of ash are Si and SiC, combined with Fig. 3, from A to F, the relative intensities of the characteristic peaks of SiC and Si were enhanced.

The XRD patterns in Fig. 3, show that characteristic peaks of carbon appear near $2\theta = 26.5°$, 42.3°, 44.5°, 50.7°, 54.6°, 59.9°, 71.5°, 77.5°, 83.6°, 85.4°, and 87.0°, with the strongest peak at 26.554°. The characteristic peaks of silicon appeared around 28.4°, 47.3°, 56.1°, 58.8°, 69.1°, 76.3°, and 88.0°, with the strongest characteristic peak at 28.443°. The peaks at 35.6°, 41.1°, 59.9°, 58.8°, 71.7°, 75.5°, and 89.9° were characteristic peaks of silicon carbide, with the strongest at 35.597°. The above results show that the main phases in the six regions of the waste graphite infusion cylinder A-F were C, Si, and SiC, and C was the main phase. Compared with the other three regions, the relative intensity of the characteristic peaks of silicon carbide in regions A and B was lower,due to the low temperature of the two regions,which result in silicon monoxide was not stable and ubstantial condensation of rising silicon vapour. Therefore, only a small amount of silicon vapor and the graphite surface reaction of the infuser a small amount of silicon carbide.Compared with the other five regions, the relative intensity of the characteristic spectral peaks of silicon carbide in region F was higher than that of silicon, which indicates that the content of silicon carbide in region F was higher than that of silicon. This was probably because the F region was the bottom of

the infusion cylinder, the closest to the heat source, that is, the location of the highest temperature, coupled with the infusion cylinder raw material isostatic graphite surface has a large number of holes, which provided passageway for the internal diffusion of the silicon liquid, As a result, the splashed silicon reacts with the graphite in this area to form a relatively large amount of silicon carbide. Based on apparent physiognomy，region D contained more impurity particles than region E, which were darker. The XRD patterns showed that region D contained more SiC than region E, possibly because region D was located in the central part of the infusion cylinder, where the upward heat flow from the silicon melt and the blowing argon gas form convection currents in this area. The enriched SiO reacts with C and CO in this region to form SiC.

During SiC formation, the reaction system should contain SiO and SiO_2. Combined with the surface of the waste graphite infusion cylinder there are earthy yellow, white scales, lumps of material, check the relevant literature, silicon monoxide at room temperature and normal pressure for the black-brown to earthy yellow amorphous powder, or white cubic, in the air when heated, earthy yellow powder into white powder[32]. In addition, silicon monoxide is not stableand oxidizes to silicon dioxide in the air.And the slow condensation of silicon monoxide vapour results in a disproportionation reaction with the products being silicon and silica. Therefore, it was inferred that the relevant substances were SiO, SiO_2, or their mixtures.

XPS was carried out to detect the substances in the six areas of the waste graphite infusion cylinder, and the results showed that the main elements in the six areas of the infusion cylinder A-F were C, Si, and O. There were three peaks of C1s, Si2p, and O1s. The results of Si2p split peak fitting are shown in Fig. 4,And the results show that there were four forms of Si element, i.e., monomorphic Si, SiC, SiO, and SiO, which were found in all six regions. These results indicate that the earthy yellow and white amorphous substances on the surface of the waste graphite infusion cylinder were SiO, SiO_2, or their mixture. It can be inferred that silica-oxygen compounds (SiO, SiO_2, or their mixtures) formed during SiC generation. The XRD did not detect SiO_2 or SiO, suggesting that amorphous SiO_2 was formed[33], which could not be detected by XRD, or that the SiO_2 content was below the detection limit.

3.3 Sample morphology and microstructure analysis

EDS showed that a large amount of Si and O composite areas(Fig. 5 (a)) existed in all six regions of the waste graphite infusion cylinder.Combined with the XPS analysis and the apparent morphology of the waste graphite infusion cylinder, it is believed that SiO, SiO_2, or their composite substances existed during SiC formation. On a micro level, there were highly-enriched areas of Si and C elements(Fig. 5 (b)) in all six regions.It is speculated that SiC may have been generated in these areas, and some special structures were observed in the corresponding areas ,as shown in Fig. 6(a, b) there are tubular and fibrous structures in the A and B regions, which are presumed to be silicon carbide in combination with EDS, with a fine particle size close to the nanoscale. Regions C and D of the graphite matrix were found to be dendrite-like silicon carbide, as shown in Figure 6 (c, d). Regions E and F, on the other hand, showed a layered structure of carbon, silicon, and silicon carbide in Figure 6 (e, f). .From a macroscopic point of view, the two regions D and E on the surface of the waste graphite infusion cylinder had larger sediment particles than region F, and the color was darker. The intensity of the characteristic peaks of SiC in the XRD patterns was higher in regions D and E than in region F, i.e., regions D and E generated more SiC. This was probably because regions D and E were located in the middle of the cylinder. The convection of the upward silicon melt heat flow with the downward argon flow, which lead to a large enrichment of SiO with CO at this location， with the strong agitation of the gas flow, a violent reaction occurs, so a large amount of SiC was generated.Regions E and F of the infusion cylinder were closer to the silicon melt, and the temperature was high, which created a more intense reaction. The splashed high-temperature silicon fluid reacts directly with the graphite of the infusion cylinder to form dense silicon carbide.

As shown in Fig. 7,samples of the waste graphite infusion cylinder from the longitudinal section were clearly divided into two layers, where the lower layer was a black graphite layer, and the upper layer was a mixture of varying thicknesses and densities of the layer. Combined with the results of the previous XRD and XPS analysis, it is presumed that the upper layer was silicon, silicon oxide, silicon monoxide, silicon

dioxide, silicon carbide, and carbon. Comparing the thickness of the upper mixture, region D was the thickest, reaching 2988.41 μm, and region B was the thinnest, only 42.43 μm. For the upper layer, from A to F, i.e., from the upper section of the infusion cylinder to the lower end, the number of pores inside the mixture gradually decreased and became smaller, which indicates that the density of the mixture was higher.

As shown in Fig. 8, regions A, B, and C all contained silicon and carbon-enriched and silicon and oxygen-enriched regions in their upper layers. Among them, the highest degree of silica-oxygen enrichment in the upper layer mixture was found in region A, which corresponds to its apparent morphology, i.e., the earthy yellow and white amorphous mixture on the surface of area A was an intermediate product formed during the generation of silicon carbide. Region B was an area with the least upper layer mixture among the six areas, as shown in the EDS elemental distribution diagrams of region B. The interfaces and the degree of silicon enrichment in regions D, E, and F were more obvious than those in regions A, B, and C.It is believed that as the temperature increased from region A to F, the thermodynamic conditions of the reaction were enhanced, and the reaction between carbon monoxide and silicon monoxide or the reaction between silicon monoxide and carbon directly to generate silicon carbide became easier. This densified the generated silicon carbide layer, and the degree of combination of silicon, silicon monoxide, and silicon carbide mixtures became higher.

3.4 Thermodynamic analysis of SiC generation in Si-C-O system during ph otovoltaic crystal pulling

Using the reaction equilibrium calculation module of HSC Chemistry thermodynamic analysis software, $\Delta_r H_m^\theta$, $\Delta_r S_m^\theta$, and $\Delta_r G_m^\theta$ of the reaction at different temperatures were calculated based on the Gibbs free energy minimum principle and entropy increase principle to analyze and discuss the spontaneity of the reaction. During silicon carbide generation, which involves the generation of intermediate products SiO (g) and CO (g) [34-35], combined with research conducted by Ding, the relevant possible reactions are as follows:

Reactions likely to produce SiO (g):

$$SiO_2(s)+C(s)=SiO(g)+CO(g) \quad (1)$$

SiO_2 (s) + CO (g) = SiO (g) + CO_2 (g) (2)

SiO_2(s)+Si(s,l,g)=2SiO(g) (3)

2Si (s,l,g)+ O_2 (g) = 2SiO (g) (4)

Reactions likely to produce CO (g):

SiO_2(s)+C(s)=SiO(g)+CO(g) (1)

CO_2(g) + C(s) = 2CO (g) (5)

SiO(g) + 2C(s) = SiC(s) + CO(g) (6)

2C(s) + O_2(g) = 2CO(g) (7)

Reactions likely to produce SiC(s):

SiO (g) + 2C (s) = SiC (s) + CO (g) (6)

SiO (g) + 3CO (g) = SiC (s) + 2CO_2(g) (8)

3SiO(g)+CO(g)=SiC(s)+2SiO_2(g) (9)

Si (s,l,g)+ C (s) = SiC (s) (10)

By calculating $\Delta_r G_m^\theta(T)$ for the possible formation of SiO (g), CO (g), and SiC (s) in the reaction temperature range of 0 ℃ to 1700 ℃ under standard conditions (P^θ = 101.325 kPa), we analyzed the relationship between changes of $\Delta_r G_m^\theta(T)$ and temperature T.

Fig. 9(a) shows the eight reactions about likely to produce SiO (g) the r elationship between changes of $\Delta_r G_m^\theta(T)$ and temperature T , in which $\Delta_r G_m^\theta$ (T) decreased upon increasing the temperature under standard conditions, except for reaction (2)Si(s,l,g)+O2(g)=2SiO(g). For Reactions (1), (2), and (3), $\Delta_r G_m^\theta$ (T) > 0 in the range of 0–1700 °C, except for reaction (3) when the silicon was in the gaseous state. For Reaction (4), $\Delta_r G_m^\theta(T) < 0$ when silicon was in the solid-liquid-gas state in the range of 0–1700 °C. Reaction (4) was most lik ely to generate gaseous silicon monoxide. However, the PV pulling graphite inf usion cylinder was under an argon atmosphere, so the oxygen content was ver y limited. The system contained large amounts of SiO_2 (s), C (s), and Si (s) a s reactants, Therefore, under the above conditions, SiO is more likely to be pr oduced by reaction (1)(SiO_2(s)+C(s)=SiO(g)+CO(g)) and reaction (3)(SiO_2(s)+Si (s,l,g) = 2SiO(g)).

Fig. 9(b) shows that during CO(g) generation, $\Delta_rG_m^{\theta}(T)$ was inversely proportional to temperature for reaction(1), reaction (5), and reaction (7) under standard conditions. $\Delta_rG_m^{\theta}(T)$ did not vary greatly with temperature for reactions (3–6) under standard conditions. Reaction (1) was not $\Delta_rG_m^{\theta}(T) < 0$ in the range of 0–1700 °C, while reactions (6) and (7) had no $\Delta_rG_m^{\theta}(T) > 0$ in the range of 0–1700 °C. Reaction (5) had a cut-off point of 700°C, and $\Delta_rG_m^{\theta}(T) < 0$ only above 700 °C. Analyzing the degree of difficulty in the occurrence of the four reactions, carbon monoxide was most likely to be generated by reaction (7). In addition, Reaction (5) and Reaction (6) were also possibleHowever, the photovoltaic crystal pulling hot field was an argon atmosphere, in which the oxygen content was very limited. Thus, CO(g) in the system should have been generated by reaction (5)($CO_2(g) + C(s) = 2CO(g)$) and reaction (6)($SiO(g) + 2C(s) = SiC(s) + CO(g)$).

As can be seen from Fig. 9(c), $\Delta_rG_m^{\theta}(T)$ for both reaction (6) and reactio n (10) in the standard state did not change much upon increasing the temperat ure, except when silicon was in the gaseous state. $\Delta_rG_m^{\theta}(T)$ for reaction (8) an d reaction (9) in the standard state increased with the temperature. For reaction (6), reaction (9), and reaction (10), $\Delta_rG_m^{\theta}(T) < 0$ in the range of 0–1700 °C. For reaction (8), $\Delta_rG_m^{\theta}(T) < 0$ up to 900 °C, and $\Delta_rG_m^{\theta}(T) > 0$ above 900 °C. Thus, SiC (g) in the system should have been generated by reaction (6)($SiO(g) +2C(s)=SiC(s)+CO(g)$), reaction (8)($SiO(g)+3CO(g)=SiC(s)+2CO_2(g)$),reaction 9($3 SiO(g)+CO(g)=SiC(s)+2SiO_2(g)$),reaction (10)($Si(s,l,g)+C(s)=SiC(s)$).

Taken together the reactions $\Delta_rG_m^{\theta}(T)$ versus temperature that are most likely to produce gaseous silicon monoxide, carbon monoxide and silicon carbide in the reaction system are shown in Fig. 9(d).

The degree of difficulty of each reaction can be derived according to Fig. 9(d), which shows that reaction (1), reaction (3), reaction (5), and reaction (6) have a great likelihood of generating intermediate products SiO(g) and CO(g). Due to the consumption of CO_2 by the graphite infusion cylinder in the system, reaction (2) can proceed in the positive direction and generate CO. Reaction (6) and reaction (10) generate SiC nuclei and also continue to generate CO. Then, the intermediate products

SiO(g) and CO(g) continue to grow on the SiC nuclei via reactions (8) and (9), and ultimately the growth of SiC is realized. Thermodynamic analysis shows that SiC was generated via a gas-solid reaction growth mechanism, where the intermediate product SiO (g) generated SiC nuclei with the infusion cylinder graphite. The intermediate reactants SiO(g) and CO(g) continued to react to grow SiC. The chemical reactions involved are as follows:

(1) SiO(g) and CO(g) generate the reaction:

$$SiO_2(s)+C(s)=SiO(g)+CO(g) \quad (1)$$

$$SiO_2(s)+Si(s,l,g)=2SiO(g) \quad (3)$$

$$C(s)+CO_2(g)=2CO(g) \quad (5)$$

(2) SiC nucleation reaction:

$$SiO(g)+2C(s)=SiC(s)+CO(g) \quad (6)$$

$$Si(s,l,g)+C(s)=SiC(s) \quad (10)$$

(3) SiC growth reaction:

$$SiO(g)+3CO(g)=SiC(s)+2CO_2(g) \quad (8)$$

$$3SiO(g)+CO(g)=SiC(s)+2SiO_2(g) \quad (9)$$

In summary, by combining the characterization results and the thermodynamic analysis, the SiC generation mechanism of the photovoltaic crystal pulling infusion cylinder is shown in Fig. 10.

From the mechanism diagram Fig. 10, during the straight pulling of monocrystalline silicon, the quartz crucible (mainly composed of silica) in the hot field reacted with the graphite torus (mainly composed of carbon) to generate SiO (g) and CO (g). The quartz crucible reacted with the silicon liquid, silicon vapor, and silicon material to generate SiO (g), and SiO (g) and CO (g) participated in the subsequent reaction as the intermediate products to generate SiC. As the silicon melt released a large amount of heat, The heat flow induces upward movement of SiO(g), CO(g), and Si(g),and argon gas blown in from the upper end of the infusion cylinder tube forms convection with the above three gases,which result in A highly enriched region of SiO(g), CO(g), and Si(g) was formed in the middle of the inflow cylinder.. In the lowermost region of the infusion cylinder, the splashing of high-temperature silicon

liquid and the infusion cylinder graphite directly reacted to generate silicon carbide. In other regions, SiO (g) and the infusion cylinder graphite reacted to generate silicon carbide nuclei and CO (g). During the generation of silicon carbide nuclei, SiO (g) and CO (g) continued to react and promote the growth of silicon carbide crystals, which generated SiO_2 (g). As the single-crystal pulling proceeded, a silicon carbide layer was generated on the surface of the infusion cylinder, and a large amount of SiO (g) and Si (g) were enriched on the silicon carbide layer. At the same time, the reaction between SiO (g) and CO (g) continued to generate silicon carbide, and a mixture of silicon, silicon monoxide, and silicon carbide was generated on the surface of the silicon carbide layer, i.e., silicon carbide was engulfed and covered.Tthe middle and lowermost part of the infusion cylinder generate the most silicon carbide, in the middle region, a large amount of enriched SiO (g), CO (g), and Si (g) reacted, and the lowermost region was due to the close proximity to the silicon melt, which had the highest reaction temperature and better thermodynamic conditions. Silicon and carbon reacted at the interface to generate a layer of silicon carbide. Due to diffusion, silicon and carbon further reacted, but the diffusion rate of carbon in β-SiC was faster than that of silicon, so silicon carbide was mainly generated on the surface of the infusion cylinder. However, because the infusion cylinder was made of isostatically-pressed graphite, there were many voids and pores in its interior, which provided conditions for the diffusion of the molten silicon to the interior of the graphite. Therefore, the interior of the graphite infusion cylinder also generated some silicon carbide, i.e., silicon carbide penetrated the interior.

4. Conclusion

Through systematic characterization and thermodynamic analysis, we elaborated the SiC generation mechanism in a PV drawn crystal waste graphite infusion cylinder. The results showed that SiO (g) and CO (g) were important reaction intermediates involved in the generation of SiC. The SiO (g) concentration was an important factor affecting the amount of SiC generation, densification, and penetration depth, in addition to temperature, air flow, and structure. SiC was not generated by a simple chemical

reaction, but the SiC generation mechanism obtained from these basic findings generally explained the apparent morphological characteristics of the waste graphite infusion cylinder. This provides theoretical guidance for prolonging the service life of the graphite infusion cylinder, improving the quality of the silicon base, and purifying and treating the waste graphite infusion cylinder. Future research should consider the potential influence of dynamics more carefully, and a detailed quantitative analysis is also necessary.

Acknowledgments

The authors are grateful for financial support from the the Major Projects of Yunnan Province (No. 202302AB080004) and the Ten Thousand Talent Plans for Young Top-notch Talents of Yunnan Province (No. YNWR-QNBJ-2020-022).

Reference

1. Chen J, Gao M, Mangla SK, Song M, Wen J (2020) Effects of technologi cal changes on China's carbon emissions. Technol. Forecast Soc Chang 153: 119938. https://doi.org/10.1016/j.techfore.2020.119938
2. Hao J, Gao F, Fang X, Nong X, Zhang Y, Hong F (2022) Multi-factor de composition and multi-scenario prediction decoupling analysis of China's ca rbon emission under dual carbon goal. Sci Total Environ. 841:156788. https: //doi.org/10.1016/j.scitotenv.2022.156788
3. Xuan D, Ma X, Shang Y (2020) Can China’s policy of carbon emission tr ading promote carbon emission reduction?. J Clean Prod 270:122383. https: //doi.org/10.1016/j.jclepro.2020.122383
4. Guo X, Dong Y, Ren D (2023) CO2 emission reduction effect of photovol taic industry through 2060 in China. Energy 269:126692. https://doi.org/10.1 016/j.energy.2023.126692
5. Jenner S, Groba F, Indvik J (2013) Assessing the strength and effectivenes sof renewable electricity feed-in tariffs in European Union countries. Energ ypolicy 52:385-401. https://doi.org/10.1016/j.enpol.2012.09.046
6. Shrimali G, Kniefel J (2011) Are government policies effective in promotin g deployment of renewable electricity resources? Energy Policy 39(9):4726– 4741. https://doi.org/10.1016/j.enpol.2011.06.055
7. Zhang L, Wang J, Wen H, Fu Z, Li X (2016) Operating performance, ind ustryagglomeration and its spatial characteristics of Chinese photovoltaic ind ustry. Renew Sust Energ Rev 65:373–386. https://doi.org/10.1016/j.rser.2016. 07.010

8. Zhao XG, Wang W (2020) Driving force for China's photovoltaic industry output growth: Factor-driven or technological innovation-driven? J Clean Prod. 274:122848. https://doi.org/10.1016/j.jclepro.2020.122848
9. Xu L, Zhang Q, Wang K, Shi X (2020) Subsidies, loans, and companies'performance: evidence from China's photovoltaic industry. Appl Energy 260: 114280. https://doi.org/10.1016/j.apenergy.2019.114280
10. Pu Y, Wang P, Wang Y, Qiao W, Wang L, Zhang Y (2020) Environmental effects evaluation of photovoltaic power industry in China on lifecycle assessment. J Clean Prod 278:123993. https://doi.org/10.1016/j.jclepro.2020.123993
11. Li J, Huang J (2020) The expansion of China's solar energy: Challenges and policy options. Renew Sust Energ Rev 132:110002. https://doi.org/10.1016/j.rser.2020.110002
12. Ballif C, Haug FJ, Boccard M, et al (2022) Status and perspectives of crystalline silicon photovoltaics in research and industry. Nat Rev Mater 7(8):597–616. https://doi.org/10.1038/s41578-022-00423-2
13. Liu Z, Sofia S, Laine HS, Woodhouse M, Wieghold S, Peters I, Buonassis iT (2020) Revisiting Thin Silicon for Photovoltaics: a technoeconomicPerspective. Energy Environ Sci 13(1):12-23. https://doi.org/10.1039/c9ee02452b
14. Szlufcik J, Sivoththaman S, Nlis J F, et al (1997) Low-cost industrial technologies of crystalline silicon solar cells. Proceedings of the IEEE 85(5): 711-730. https://doi.org/10.1109/5.588971
15. Li B, Wu C, Xu J, Hu D, Zhang T, Fang X, Tong J (2020) One-pot redox synthesis of graphene from waste graphite of spent lithium ionbatteries with peracetic acid assistance. Materials Chemistry and Physics. 241, 122397. DOI: 10.1016/j.matchemphys.2019.122397
16. Ding S, Sun S, Xu H, Yang B, Liu Y, Wang H, Zhang R (2019) Preparation and adsorption property of graphene oxide by using waste graphite from diamond synthesis industry. Mater Chem Phys 221:47-57. https://doi.org/10.1016/j.matchemphys.2018.09.036
17. Jalili R, Esrafilzadeh D, Aboutalebi SH, Sabri YM, Kandjani AE, Bhargava SK,Wallace GG (2018) Silicon as a ubiquitous contaminant ingraphene derivatives with significant impact on device performance. Nat Commun 9(1):5070. https://doi.org/10.1038/s41467-018-07396-3
18. Jara AD, Betemariam A, Woldetinsae G, Kim JY (2019) Purification, application and current market trend of natural graphite: A review. Int J Min Sci Technol 29(5):671-689. https://doi.org/10.1016/j.ijmst.2019.04.003
19. Zhang J, Liu D, Pan Y (2020) Suppression of oxygen and carbon impurity deposition in the thermal system of Czochralski monocrystalline silicon. J Semicond 41(10):102702. https://doi.org/10.1088/1674-4926/41/10/102702
20. Liu D, Zhao XG, Zhao Y (2017) A review of growth process modelingand control of Czochralski silicon single crystal. Control Theory Appl 34(1):1-12. https://doi.org/10.7641/CTA.2017.60247
21. Li X, Lei Y, Qin L, Han D, Wang H, Zhai D, Kan F (2021) Mildly-Expa

nded Graphite with Adjustable Interlayer Distance as High-Performance An ode for Potassium-Ion Batteries. Carbon 172:200-206. https://doi.org/10.1016 /j.carbon.2020.10.023
22. Liu X, Gao B, Kakimoto K (2015) Numerical investigation of carbonconta mination during the melting process of Czochralski silicon crystal growth. J Cryst Growth 417:58–64. https://doi.org/10.1016/j.jcrysgro.2014.07.040
23. Kalejs JP, Chalmers B (1986) Melt-interface mechanism for generation ofsil icon carbide microdefects in silicon. J Cryst Growth 79(1-3):487–492. https: //doi.org/10.1016/0022-0248(86)90481-1
24. Ouaddah H, Regula G, Reinhart G, Périchaud I, Guittonneau F, Barrallier L, Mangelinck-Noël N (2023) Crystal distortions and structural defects at s everal scales generated during the growth of silicon contaminated with carb on.Acta Mater 252:118904. https://doi.org/10.1016/j.actamat.2023.118904
25. Bornside, DE, Brown RA, Fujiwara T, Fujiwara H, Kubo T (1995) TheEff ects of Gas-Phase Convection on Carbon Contamination of Czochralski-Gro wn Silicon. J Electrochem Soc 142(8):2790. https://doi.org/10.1149/1.205009 4
26. Camel D, Cierniak E, Drevet B, Cabal R, Ponthenier D, Eustathopoulos N (2020) Directional solidification of photovoltaic silicon in re-useable graphit e crucibles. Sol Energy Mater Sol Cells 215:110637. https://doi.org/10.1016/ j.solmat.2020.110637
27. Heilbronn L, Townsend L, Burnham C, Green H, Tsai PE, Borak T, McBe th R(2014) Neutron fluences and doses behind shielded environments in sp ace. 2014 IEEE Aerospace Conference 2014:1-8. https://doi.org/10.1109/AER O.2014.6836309
28. Belouet C, Monville M, Bigot C, Jolivet E, Varrot R, Chancolon J, Bonna my S (2018) The carbon substrate in RST Si ribbon technology for solar cells. Carbon 141:427-443. https://doi.org/10.1016/j.carbon.2018.09.049
29. Delannoy Y, Barvinschi F, Duffar T (2007) 3D dynamic mesh numerical m odel for multi-crystalline silicon furnaces. J Cryst Growth 303(1):170–174. https://doi.org/10.1016/j.jcrysgro.2006.12.075
30. Gao B, Chen XJ, Nakano S, Kakimoto K (2010) Crystal growth of high-p urity multicrystalline silicon using a unidirectional solidification furnace fors olar cells. J Cryst Growth 312(9):1572–1576. https://doi.org/10.1016/j.jcrysgr o.2010.01.034
31. Zheng L, Ma X, Hu D, Zhang H, Zhang T, Wan Y (2011) Mechanism an dmodeling of silicon carbide formation and engulfment in industrial silicon directional solidification growth. J Cryst Growth 318(1):313–317. https://doi. org/10.1016/j.jcrysgro.2010.11.141
32. Lee JI, Lee KT, Cho J, Kim J, Choi NS, Park S (2012) Chemical-assisted thermal disproportionation of porous silicon monoxide into silicon-basedmult icomponent systems. Angew Chem 124(11):2821-2825. https://doi.org/10.100 2/ange.201108915
33. Wang L, Liu B, Li H, Yang W, Ding Y, Sinogeikin SV, Mao WL (2012)

Long-range ordered carbon clusters: a crystalline material with amorphous building blocks. Science 337(6096):825-828. https://doi.org/10.1126/science.1220522

34. Chen J, Zhang J, Wang M, Li Y (2014) High-temperature hydrogen sensor based on platinum nanoparticle-decorated SiC nanowire device. Sens Actuat or B-Chem 201:402-406. https://doi.org/10.1016/j.snb.2014.04.068
35. Wang MM, Chen JJ, Liao X, et al (2014) Highly efficient photocatalytichy drogen production of platinμm nanoparticle-decorated SiC nanowires under simulated sunlight irradiation. J Hydrog Energy 39(27):14581-14587. https://doi.org/10.1016/j.ijhydene.2014.07.068

* Ethics approval and consent to participate

We don't cover ethics approval and consent to participate.

* Consent for publication

Not applicable.

* Availability of data and materials

All data generated or analysed during this study are included in this published article.

* Competing interests

The authors declare that they have no competing interests.

* Funding

The authors are grateful for financial support from the the Major Projects of Yunnan Province (No. 202302AB080004) and the Ten Thousand Talent Plans for Young Top-notch Talents of Yunnan Province (No. YNWR-QNBJ-2020-022).

* Authors' contributions

Yiyou Hu: Conceptualization, Resources, Writing - review & editing, Visualization, Validation, Supervision. **Zhengjie Chen:** Conceptualization, Methodology, Validation, Formal analysis, Investigation, Data curation; **Yonghang Zhang:** Methodology, Formal analysis, Data curation ;**Xiuhua Chen:**Conceptualization, Investigation, Validation;**Wenhui Ma:** Formal analysis, Validation, Data curation.

* Authors' information (optional)

Yiyou Hu[1,2], Zhengjie Chen[1,2,3*], Yonghang Zhang[1,2,3], Xiuhua Chen[4], Wenhui Ma[1,2,3]

[1] Faculty of Metallurgical and Energy Engineering, Kunming University of Science and Technology, Kunming 650093, China;

[2] State Key Laboratory of Complex Nonferrous Metal Resources Cleaning Utilization in Yunnan Province, Kunming University of Science and Technology, Kunming 650093, China;

[3] The National Engineering Laboratory for Vacuum Metallurgy, Kunming University of Science and Technology, Kunming 650093, China;
[4] The School of Materials and Energy, Yunnan University, Kunming 650093, China;
*Corresponding author
E-mail address: czjkmust@126.com(Z. Chen)

* Disclosure of potential conflicts of interest

We declare that we have no conflict of interest.

* Research involving Human Participants and/or Animals

Not applicable.

* Informed consent

Not applicable.

Table Captions

Table 1 Fixed Carbon Detection Data

Table 1

samples	A	B	C	D	E	F
Fixed carbon	95.85%	91.44%	72.00%	58.19%	74.32%	52.41%

Figures

Fig. 1

Fig. 2

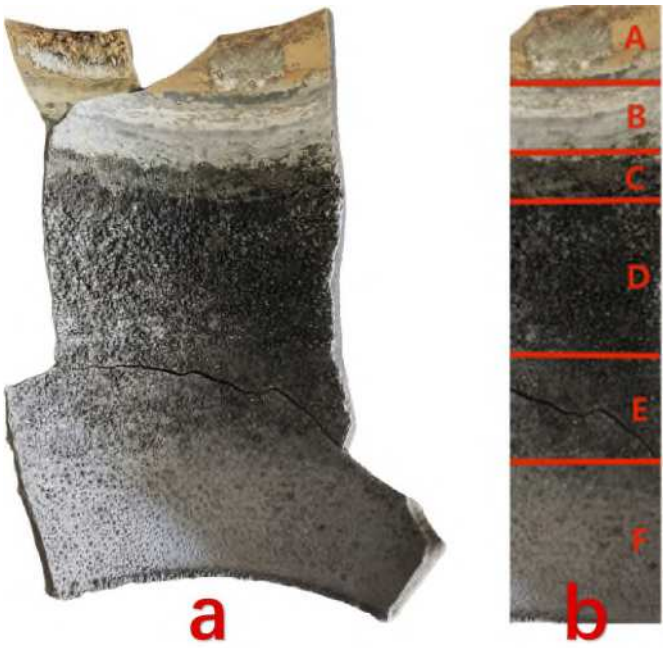

Fig. 3

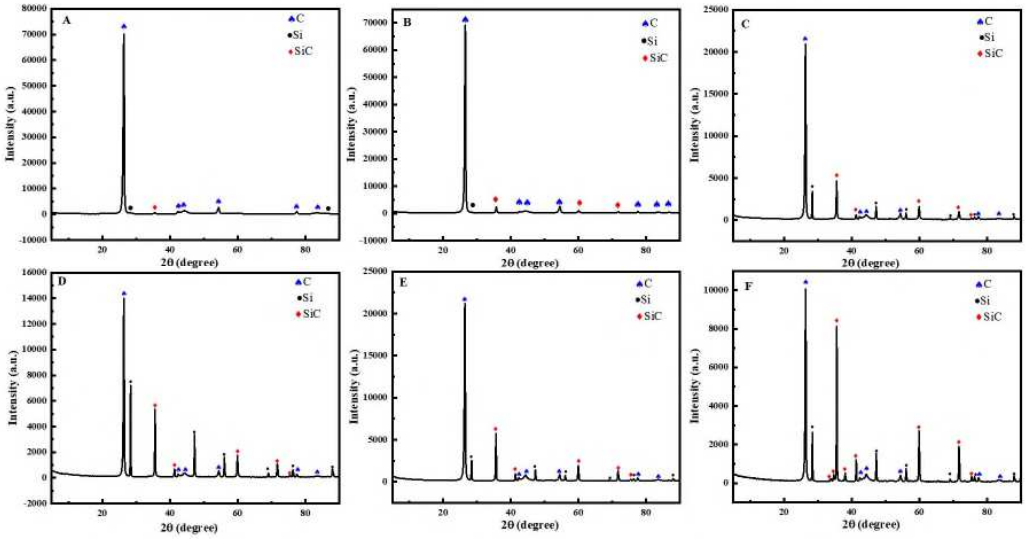

Fig. 4

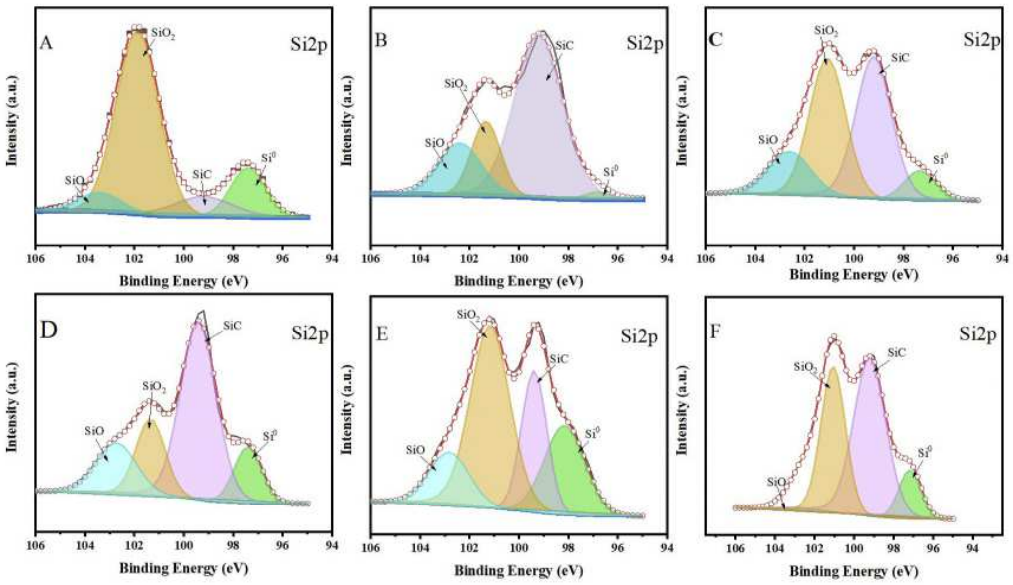
A
Si2p
SiO2
SiO
SiC
Si0
B
Si2p
SiC
SiO2
SiO
Si0
C
Si2p
SiO2
SiC
SiO
Si0
D
Si2p
SiC
SiO2
SiO
Si0
E
Si2p
SiO2
SiC
SiO
Si0
F
Si2p
SiO2
SiC
Si0
Intensity (a.u.)
Binding Energy (eV)
106
104
102
100
98
96
94

Fig. 5

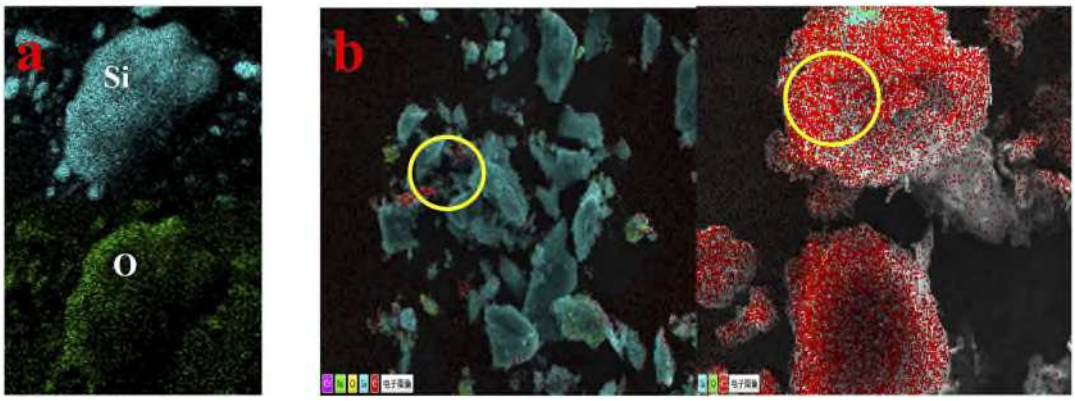

Fig. 6

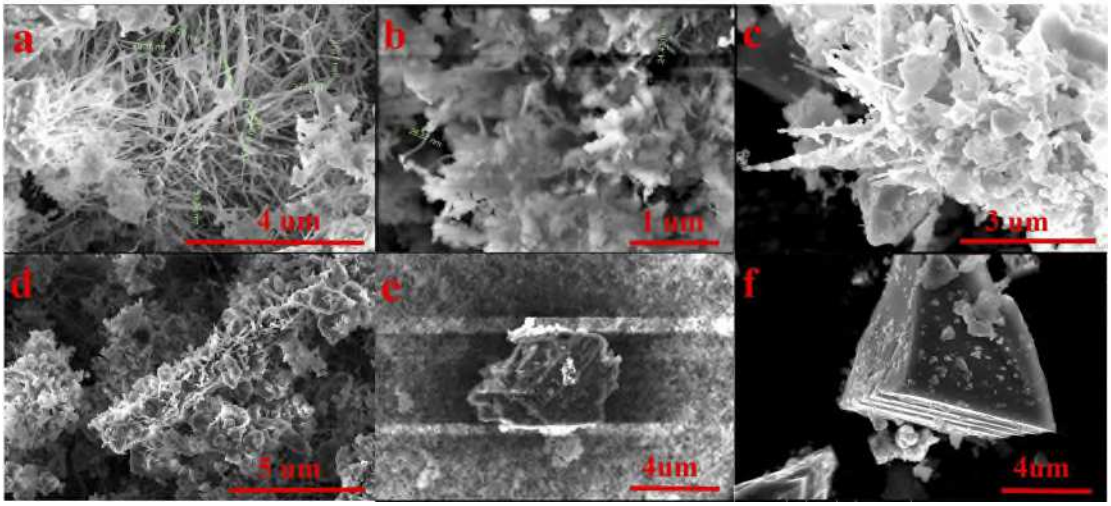

Fig. 7

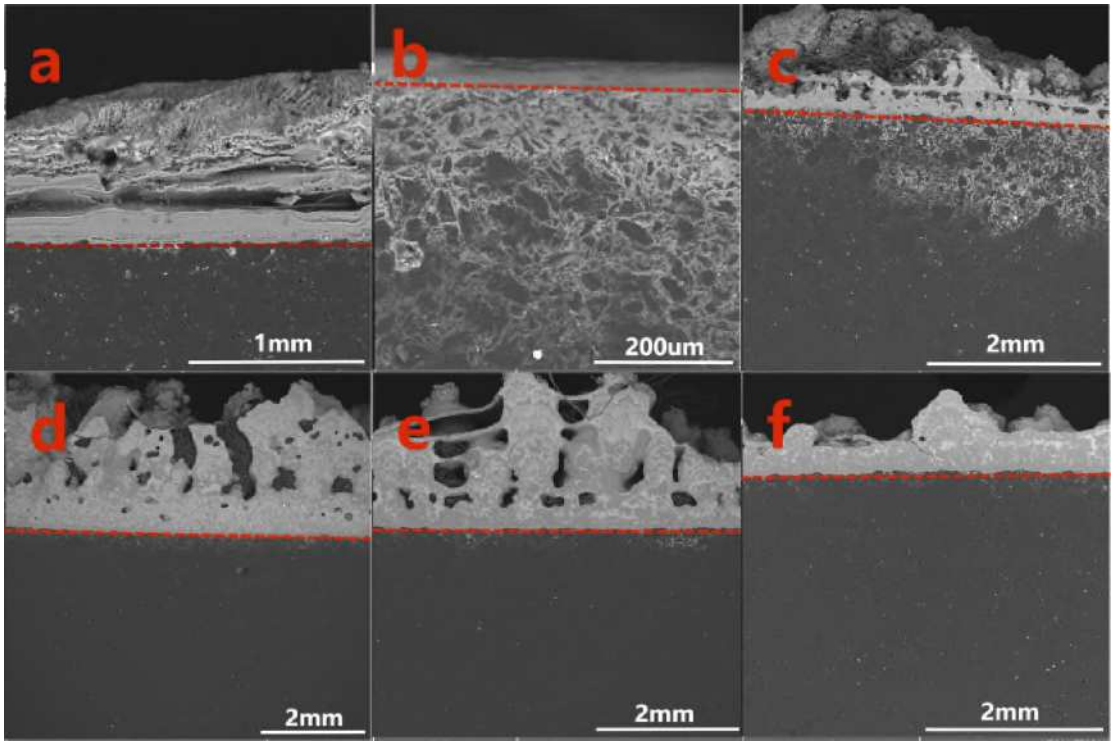

Fig. 8

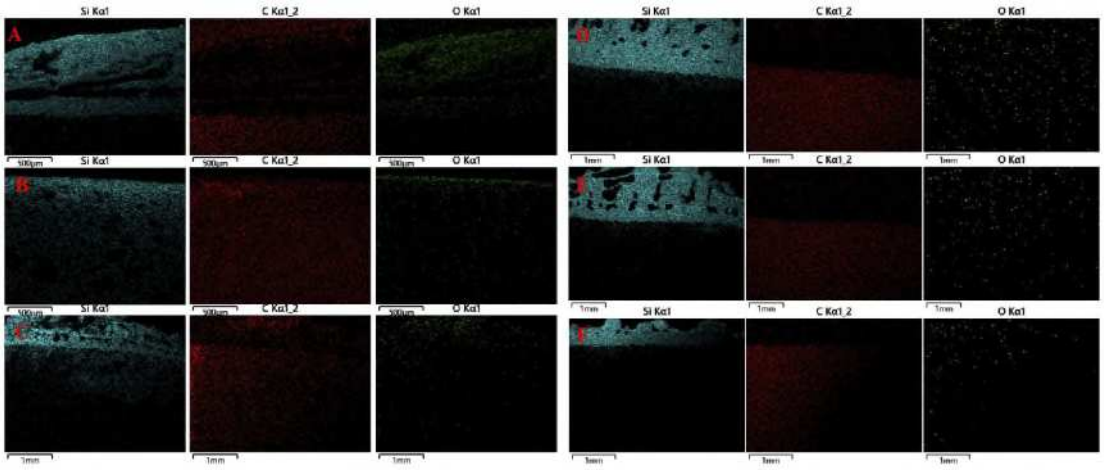

Fig. 9

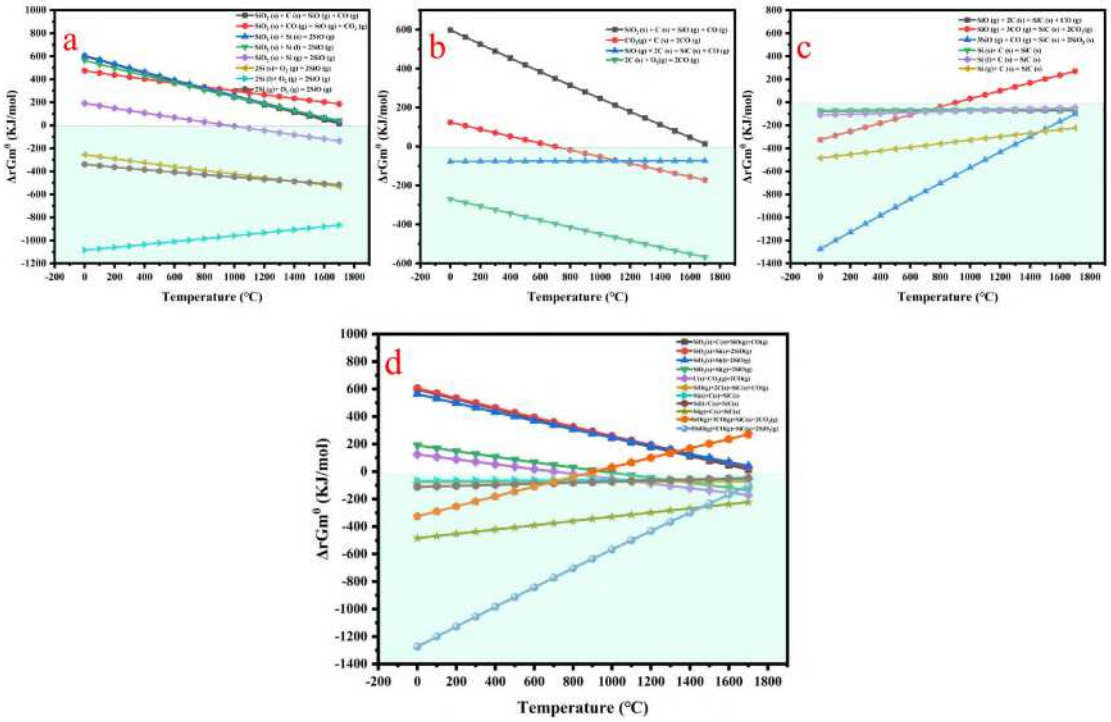

Fig. 10

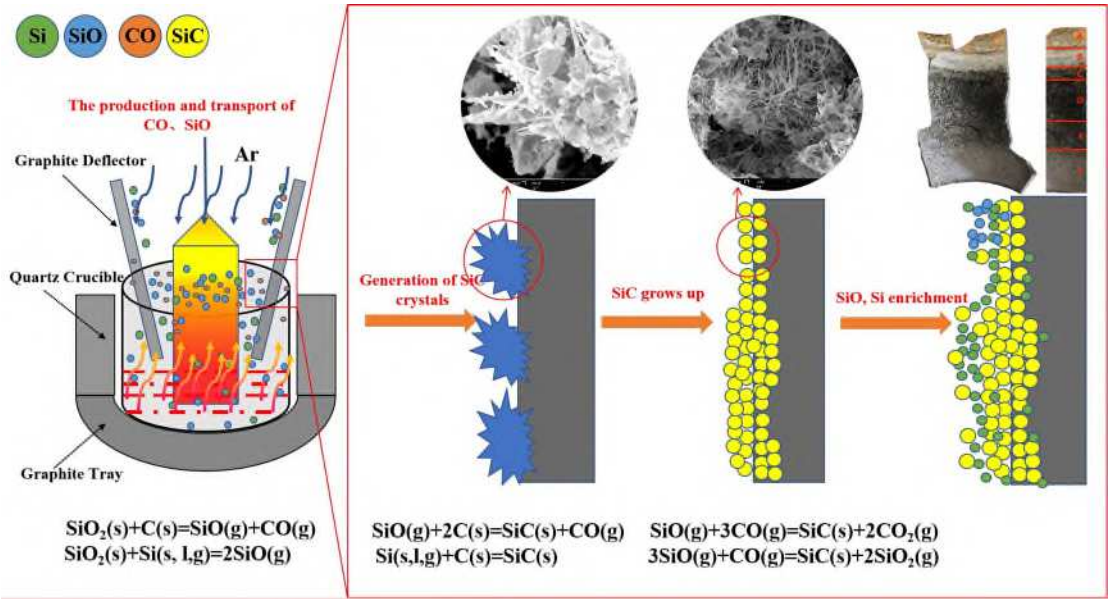
Si
SiO
CO
SiC
The production and transport of CO、SiO
Ar
Graphite Deflector
Quartz Crucible
Graphite Tray
Generation of SiC crystals
SiC grows up
SiO, Si enrichment
SiO2(s)+C(s)=SiO(g)+CO(g)
SiO2(s)+Si(s, l,g)=2SiO(g)
SiO(g)+2C(s)=SiC(s)+CO(g)
Si(s,l,g)+C(s)=SiC(s)
SiO(g)+3CO(g)=SiC(s)+2CO2(g)
3SiO(g)+CO(g)=SiC(s)+2SiO2(g)

Supplementary Files

This is a list of supplementary files associated with this preprint. Click to download.

- Supplementarymaterial.docx